

FEM modeling based on molecular results for PE/SWCNT nanocomposites

A. M. Fattahi ^{1*}, S. Roozpeikar ², N. A. Ahmed ¹

¹ Department of Mechanical Engineering Science Department, Faculty of Engineering and Built Environment, University of Johannesburg, 2006, South Africa

² Department of Mechanical Engineering, Tabriz Branch, Islamic Azad university, Tabriz, Iran

*Corresponding author E-mail: afattahi@uj.ac.za

Abstract

This study aimed to evaluate the mechanical properties of single walled carbon nanotube (SWCNT) reinforced composites using 3-D representative volume element (RVE). Then, RVE was created by finite element method using ABAQUS software. By using the results of atomic modeling, fiber and matrix interface properties were extracted and then a model for predicting the elastic modulus of nanocomposites was presented. Also, the longitudinal elastic module of Polyethylene/ CNT nanocomposite was computed and compared with experimental results. Load transfer conditions between CNTs and matrix were modeled using a separated interfacial region. Numerical examples using FEM were presented. Based on the modeling results, the increase of weight fraction of nanotubes led to the increase of equal elastic modulus of nanocomposite. By increasing the volume fraction of CNTs in the experiments, the dispersion of particles was much more difficult and the empirical results of elastic modulus were lower than those predicted by finite element software.

Keywords: FEM; CNT; Elastic Modulus; Continuum Mechanic Model; RVE.

1. Introduction

Since polymers reinforced with carbon nanotubes (CNTs) have become very popular in different fields such as aerospace, automotive, wind turbines and packaging, calculation and modeling of their mechanical behaviors have attracted many researchers. Qian et al. [1] showed that the hardness and tensile strength of a polymer was increased by 36-42% and 25%, respectively, with the addition of 1% CNTs into its matrix. It has also been shown by experimental studies and atomic modeling that CNTs had very high moduli and strengths of 300-1000 GPa which were obviously higher than those of carbon fibers [2,3]. Other important properties of these materials include high geometrical ratios as well as high strength to weight and hardness to weight ratios. Thostenson et al. [4] found that nanocomposites with the abovementioned properties could be obtained and optimally employed by the addition of CNTs into some matrices. Recently, polymer supports have been more popular but other materials such as different metals and ceramic are also being used. CNTs are widely used in the production of nanocomposites due to their homogeneous distribution characteristic. Improving the mechanical properties of composites relies on load transmission mechanism between fiber and matrix. If the cohesion of fiber and matrix too weak to tolerate high loads, high tensile strength of CNTs becomes useless. Safaei et al. [5] studied the elastic transition of platelet reinforced composites using Finite Element Method. It has been reported that some polymers have very high surface cohesion. Andrews et al. [6] fabricated MWCNTs composites using shear mixing method and observed a 15% increase in their tensile moduli by the addition of 5% MWCNTs. Determination of electrical, mechanical, and thermal properties of materials is very important in the manufacturing and designing of modern and sandwich nanocomposites. Safaei et al. [7, 8] analyzed the forced and free vibrations of

nanocomposite sandwich plates under thermo-mechanical loadings. Molecular dynamics modeling is inefficient in analyzing nanocomposites with high lengths and long time scales and therefore, in these types of problems, continuum mechanics method is preferred. This method have been successfully used in the mechanical modeling of CNTs which could be in thin shell, beam, or solid cylinder modes [9-10]. Lia et al. [11] introduced a solid 3D model for CNTs-reinforced composites with complete accuracy and compatibility between CNTs and matrix. The mechanical properties of nanocomposites have also been studied using continuum mechanics and RVE methods [12-15]. The efficiency of these nanocomposites re affected by many factors among the most important of which is the load transfer mechanism of from matrix to CNTs. Many studies have been performed on CNTs and FG [16, 17], piezoelectric [18] and nano materials [19]. Sahmani et al. [20-22] studied size dependent and nonlocal theory via shear deformation method in thermal environments and used molecular dynamics simulations for the analysis of biaxial instability in 3D metallic carbon nanosheets [23]. In another work, Samhain et al. [24, 25] employed nonlocal anisotropic shear deformable plate model to study uniaxial instability of 3D metallic and nonlinear axial instability of zirconia nanosheets. In the last decade, sandwich structures and their properties have attracted many researchers due to their unique properties. Huang et al. [26-29] evaluated the vibration and damping mechanisms of sandwich structures with elastic-viscoelastic-elastic core. Moradi et al. [30-32] showed the effects of CNTs and clusters in sandwich nanocomposites as well as their vibrations and buckling via a mesh free method.

Due to unique thermal, mechanical, and electrical properties of CNTs, development of these nano-scale particles can incorporate favorable properties into a material. Najipour et al. [33] studied post-buckling behavior of FGM nanoparticles based on surface elasticity theory. In another work, they investigated the mechanical

properties of PE/CNT composites. More recently, CNTs have been theoretically and experimentally investigated as reinforcing fibers to determine the electrical and mechanical characteristics of CNTs-based composites [34-51].

In this work we evaluated the mechanical properties of SWCNTs-reinforced composites using 3-D RVE. Then, we simulated its elastic behavior by creating RVE using finite element method. Based on atomic modeling results, the properties of fiber and matrix interface were extracted and a model was developed for the prediction of the elastic moduli of e nanocomposites. Also, the longitudinal elastic modulus of polyethylene/ CNTs nanocomposites were calculated and compared with experimental results.

2. Problem statement and assumptions

The effect of the addition of CNTs on different matrices including polymer have been widely investigated and different analytical and numerical methods have been used to evaluate nanocomposite behaviors among which finite element method has attracted great attention. The main goal of this work was to develop a modeling technique for the determination of the properties of nanocomposites and obtain the required equations to extract the results from finite element software. In this work, we also evaluated and extracted the interface properties of CNTs. The effect the addition of CNTs to four different matrices with different elastic moduli was investigated by modeling. Then, elastic nanocomposite model was used to examine the effect of the addition of reinforcer to polyethylene matrix. In this work, we assumed that the CNTs and matrix within RVE were elastic continuum, isotropic, and homogenous and their Young's moduli and Poisson's ratios were known. Also, for the simulation of CNTs/matrix interface, an individual section was created and its properties were determined with atomic simulations [34]. Finally, we compared and validated simulation results with experimental results [33].

3. Finite element modeling approaches

3.1. General

According to Fig. 1, the elements used in the modeling for the matrix and CNTs were 3D tension elements of C3D8R and for the interface was adhesive element of COH3D8.

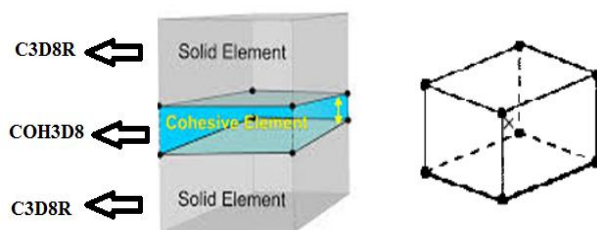


Fig. 1: The Elements Used in the Model

To achieve the properties affecting nanocomposites reinforced with CNTs, cylindrical RVE (Fig. 2) was used in the simulation of a SWCNTs in a matrix and 3D modeling was employed for two cases of short and long CNTs.

The interface between CNTs and matrix is the most important region in investigating the possibility of tension transfer and other properties of nanocomposites. In different studies, as the primary assumption, the bond between CNTs and matrix is assumed to be complete in analyses based on continuous media. But to make simulations more realistic, spring elements were used to model the interface. In this work, an intermediate phase with low thickness has been modeled in the simulation of interface and to determine its properties, the results obtained from atomic modeling were used. To define the region of interface and assign certain properties to it, we had to create a separate region in the form of a tube. The application of a separate physical section did not mean the existence of

a phase or third material between CNTs and polymer and this model was only a type of assimilation for modeling force transfer properties from matrix to CNT.

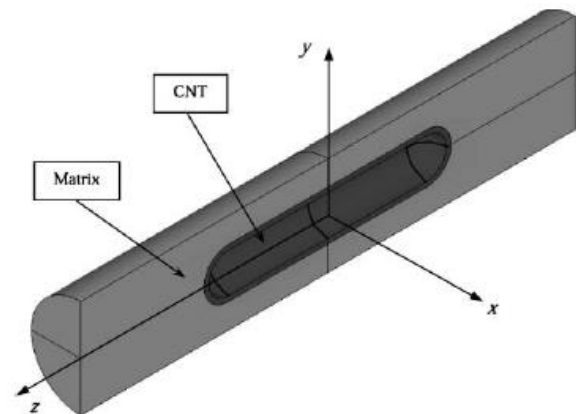


Fig. 2: Cross-Sectional View of a Cylindrical RVE

In this work, the atomic simulation results of Namilae et al. [34] was used for determining interface properties. A 0.05 displacement was applied on terminal atoms of CNTs whose primary lengths were 15 Å. For each displacement, system was balanced for 150 time interval of 0.2 Fs. These simulations were performed until some hydrocarbon chains were disintegrated and were generally lasted for 500000 to 800000 time intervals.

Fig. 3 shows the fitted stretching-separation diagram in the mentioned research in which the slope of primary section gives hardness to length unit of the interface.

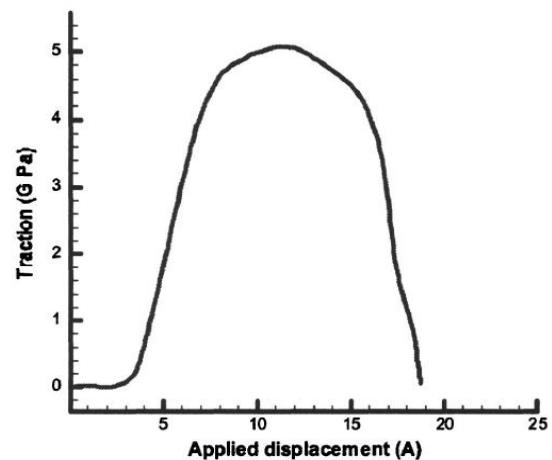


Fig. 3: Traction-Displacement Plot Obtained From Atomic Simulation

$$M = \frac{(0.1 - 0)}{(3 - 0)} = 0.03333 \text{ GPa} / \text{Å} \quad L_{CNT} = 122 \text{ Å} \quad (1)$$

where L_{CNT} is the length of CNT element. Since molecular dynamics have been employed, the length of CNT was assumed to be 122 Å. By multiplying this number by the slope of diagram, interface hardness was obtained which was directly input into ABAQUS software.

$$E_z = m \times L_{CNT} = 0.03333 \times 122 = 4.06 \text{ GPa} \quad (2)$$

Interface properties were extracted for the primary section of the diagram until 5 Å displacement. This selection seemed reasonable for the maximum displacement of 0.5 nm which has been applied to all models in this research. Poisson's coefficient and thickness of interface were 0.3 and 0.4 nm, respectively.

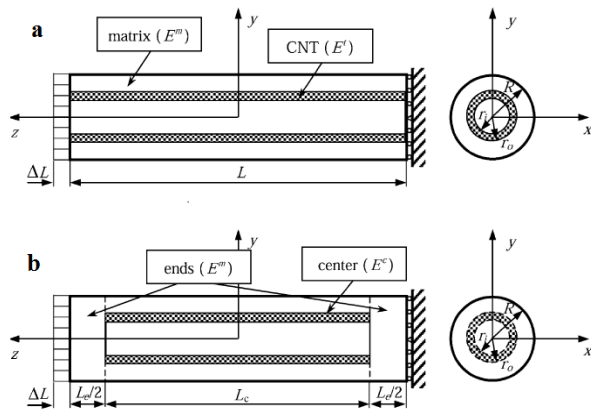


Fig. 4: Nanocomposite Unite Cell Under Axial Loading with a) Long and b) Short CNT.

A Long carbon nanotube inside the RVE is shown in Fig. 4-a. Its sizes and properties are summarized in Table 1

Table 1: Dimension and Properties of RVE long CNT

Properties	Intermediate phase	Matrix	CNT fibre
Length (nm)	100	100	100
Internal radius (nm)	5	10	4.6
Outer radius (nm)	5.4		5
Elastic modulus (GPa)	4.06	5, 20, 100, 200	1000
Poisson's coefficient	0.3	0.3	0.3

The applied load was a displacement load which had been applied on to the surface of volume element. Longitudinal elastic modulus of composite was calculated using Eq. (3)

$$E_z = \frac{\sigma_z}{\epsilon_z} = \frac{L}{\Delta L} \sigma_{ave} \quad (3)$$

The model considered for short CNT in matrix is shown in Fig. 4-b. Its sizes and properties are summarized in Table 2.

Table 2: Dimension and Properties of RVE with Short CNT

Properties	Intermediate phase	Matrix	CNT fibre
Length (nm)	100	100	50
Internal radius (nm)	5	10	4.6
Outer radius (nm)	5.4		5
Elastic modulus (GPa)	4.06	5, 20, 100, 200	1000
Poisson's coefficient	0.3	0.3	0.3

3.2. Polyethylene/CNTs nanocomposite RVE

3.2.1. Long carbon nanotube inside the RVE

In this section the reinforcing effect of CNTs in polyethylene matrix for different weight fractions have been investigated (Table 3).

Table 3: Properties of RVE with Polyethylene Matrix

Properties	Intermediate phase	Matrix	CNT fibre
Length (nm)	150		150
Internal radius (nm)	5	Changes with x	4.6
Outer radius (nm)	5.4		5
Elastic modulus (GPa)	4.06	2.020	1000
Poisson's coefficient	0.3	0.3	0.3
Density (g/cm ³)	--	0.94	1.68

To change the parameter of weight fraction, a symmetric model, according to Fig. 5, was developed such that we could change x parameter to achieve different volume and weight fractions and study the effect of the addition of CNTs.

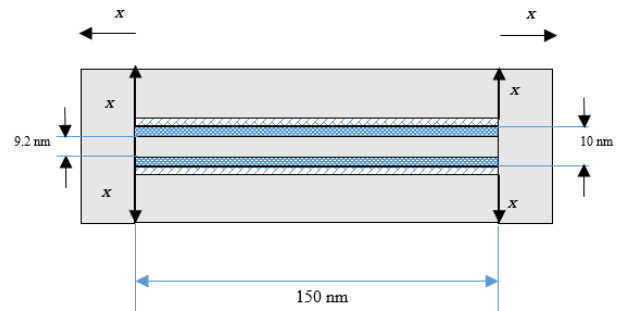


Fig. 5: Schematic of Polyethylene/CNT Nanocomposite

The volume of CNT and the volume of RVE element were calculated as follows:

$$V_{CNT} = \pi((5)^2 - (4.6)^2) \times (150), V_{RVE} = \pi\left(\frac{2x+10}{2}\right)^2 \times (2x + 150) \quad (4)$$

Weight fraction was also calculated as:

$$V_f = \frac{V_{CNT}}{V_{RVE}} = \frac{w_f}{w_f + \left(\frac{\rho_f}{\rho_m}\right)(1-w_f)} \quad (5)$$

where $\rho_f = 1.68 \text{ g/cm}^3$ is the density of CNTs, $\rho_m = 0.94 \text{ g/cm}^3$ is the density of matrix, and w_f is the weight fraction of fiber. Then, for each certain volume fraction, the value of x could be obtained by solving the third order equation of (6):

$$V_{RVE} = \frac{V_{CNT}}{V_f} \times 100 = \pi\left(\frac{2x+10}{2}\right)^2 \times (2x + 150) = \frac{\pi\left(\frac{10}{2}\right)^2 - \pi\left(\frac{9.2}{2}\right)^2 \times 150}{V_f} \times 100 \quad (6)$$

According to Fig. 5, the length and diameter of RVE element were calculated using the following equations in terms of nm:

$$DRVE=2x+10, LRVE=2x+150 \quad (7)$$

To comply with the results of [33], volume fraction was considered to be 0.5, 1 and 1.5 % and the value of x was obtained by solving the equation and by having the value of x for each volume fraction, the dimensions of RVE were obtained. Table 4 shows the obtained results.

Table 4: Dimensions of RVE for Various Weight Fraction

Weight fraction	Volume fraction	Length of RVE (nm)	Diameter of RVE (nm)	Parameter x (nm)
0.5	0.280	203.56	63.56	26.78
1	0.562	186.8	46.8	18.4
1.5	0.845	179.08	39.08	14.54

The results obtained from FEM and mixture law are summarized in Table 5. Due to axial loading, FEM results were totally close to those of mixture law. But generally, due to the nano scale and complexity of interface in nanocomposites reinforced with CNTs, strength rules of materials do not provide correct results in the evaluation of the properties of these materials and therefore, by modeling the interface as adhesive region model, more realistic values could be obtained which were smaller than those obtained by complete bonding and mixture law. The results obtained from adhesive region model showed that by adding 5% v/v CNTs into different matrices with elastic modulus of 5 to 200 GPa, the longitudinal elastic modulus of nanocomposites were increased to 1.14 to 10.62 times their initial values.

In Figs. 6 and 7, it can be seen that the effect of the addition of 5% v/v CNTs into polymer matrices was more significant on matrices with lower hardness where the ratio of longitudinal elastic modulus of composite to elastic modulus of matrix was increased to more than 10 times.

Normal stress contour for 3D model of nanocomposites reinforced with long CNTs under axial loading for $\frac{E_f}{E_m} = 200$ is shown in Fig. 8.

Table 5: Longitudinal Elastic Modulus for Nanocomposites Reinforced with Long Fiber

E_m	Rule of Mixture	FEM/Complete bonding	FEM/cohesive zone model
200	1.1948	1.1985	1.1456
100	1.4384	1.4421	1.3891
20	3.3866	3.3849	3.3353
5	10.6925	10.6575	10.6275

Note: Long CNT, $E_f=1000$ GPa, thickness=0.4 nm, volume fraction=0.04871, 3D /modelling

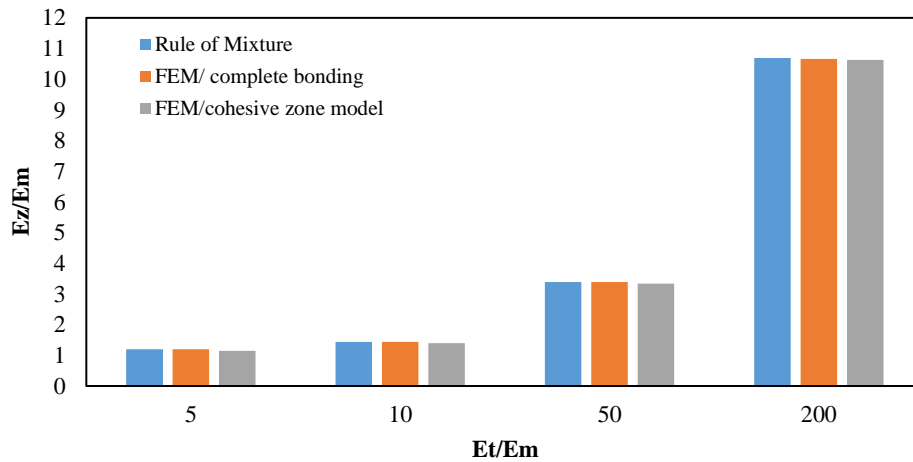


Fig. 6: Variations of Elastic Modulus of Nanocomposites Reinforced with Long CNTs in Different Matrices

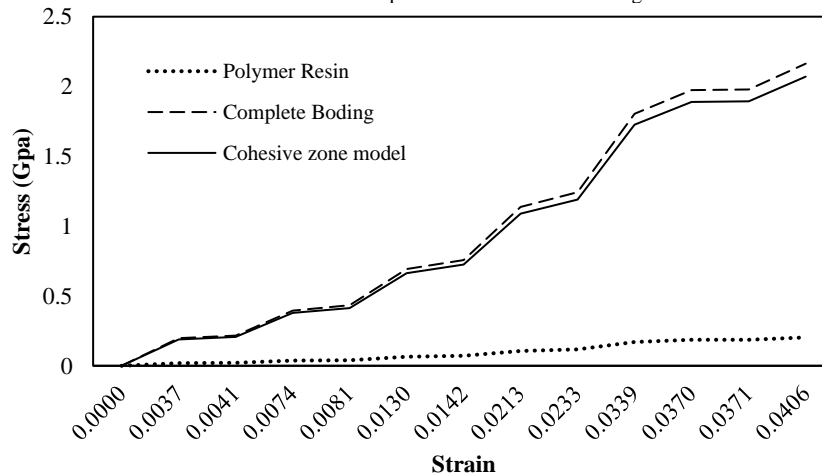


Fig. 7: Stress-Strain Diagram for Polymer/Long CNTs Composite (Volume Fraction of 5%)

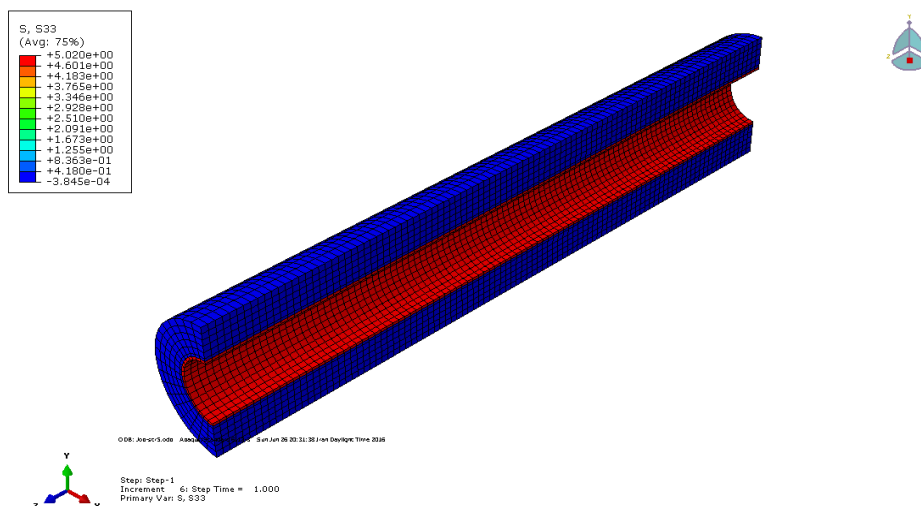


Fig. 8: Stress Transfer in Nanocomposites Reinforced with Long CNTs for $E_t/E_m=200$

Also, to determine the reinforcement capacity of CNTs, stress diagrams along the radius of RVE containing long CNTs for different matrices are depicted in Fig. 9. The highest stress transfer occurred in polymer matrix with $E_m=5$ GPa and for matrices with higher hardness, the difference of matrix and fiber stress was lower.

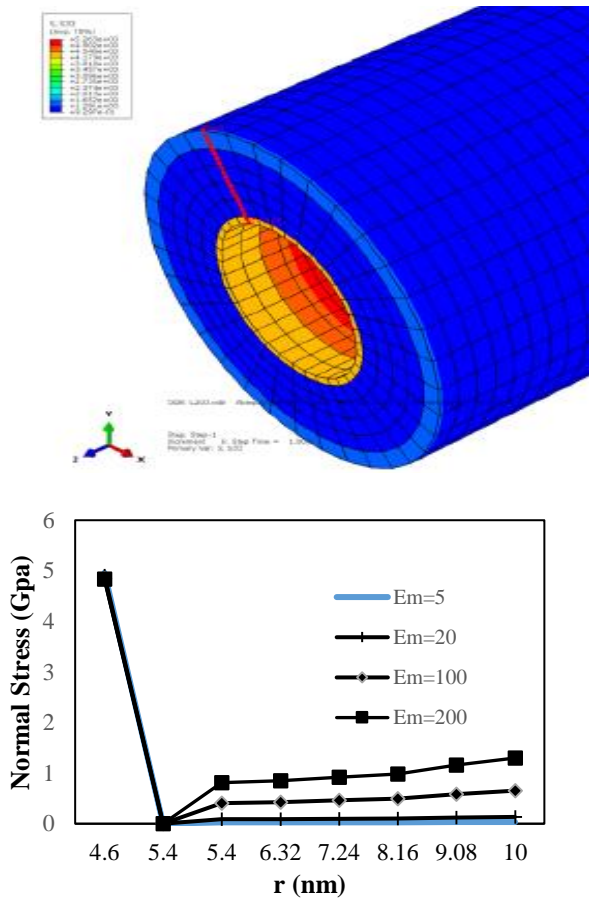


Fig. 9: Normal Stress Variation Along the Radius of RVE Containing Long CNTs at $L=100$ Nm

3.2.2. Short carbon nanotube inside the RVE

According to Fig. 10, cylindrical RVE containing short CNTs located at the center of RVE was created in ABAQUS software and the displacement of 0.5 nm was applied to the free surface of volume element.

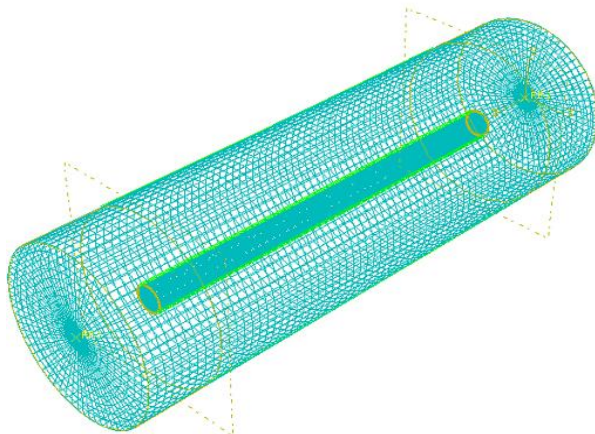


Fig. 10: RVE of Nanocomposite Reinforced with Short CNTs

FEM and mixture rule results are summarized in Table 6. The results showed that by adding 2% v/v CNTs, the longitudinal elastic modulus of nanocomposites containing matrices with lower hardness were increased more significantly and for $\frac{E_f}{E_m} = 5$, CNTs did not have reinforcement effect and elastic modulus of the nanocomposite was decreased. The reason for this was that, due to the lower fraction of CNTs, its high strength could not compensate the shortage of CNTs in this formulation.

Table 6: Longitudinal Elastic Modulus for Nanocomposites Reinforced with Short Fiber

E^m	Rule of Mixture	E_z/E_m	
		FEM/ Complete bonding	FEM/cohesive zone model
200	0.9701	0.9617	0.9386
100	1.0628	1.0471	1.0258
20	1.4550	1.3561	1.3329
5	1.7879	1.5677	1.5287

Short CNT, $E_f=1000$ GPa, thickness=0.4 nm, volume fraction=0.0211, 3D modeling

Like long fibers, in case of reinforcement with short fiber also the modeling of interface and providing adhesive region model can result in more realistic and lower values of elastic modulus for nanocomposites compared to complete bonding and mixture law.

According to Figs. 11 and 12, by adding 2% v/v CNTs into matrix polymer, elastic modulus of the nanocomposite was increased to 1.52 times but for metal matrix with Young's modulus of 200 GPa, the ratio of E_z/E_m was below 1 and low volume fraction of short CNTs could not compensate the lost material and reinforcement effect.

Normal stress contour of σ for 3D model of nanocomposite reinforced with short CNTs under axial loading for $\frac{E_f}{E_m} = 200$ is shown in Fig. 13.

Stress diagram along the radius of RVE containing short CNTs for two sections of $z=100$ nm and $z=75$ nm for different matrices are depicted in Fig. 14. As can be seen, average stress was decreased in radial direction from fiber to the end of matrix.

The effect of the addition of long and short CNTs on the longitudinal elastic modulus of the nanocomposites with different matrices are shown in Fig. 15. The obtained results showed that the reinforcement of short CNTs fibers was not as effective as that of long CNTs and this was more obvious for polymer matrices with lower hardness such that the longitudinal elastic modulus of nanocomposites with long fibers were about 7 times that of those with short fibers.

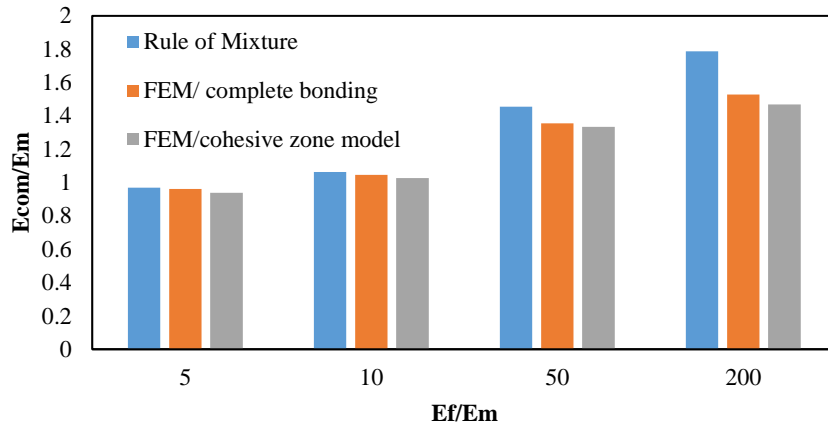


Fig. 11: Variations of Elastic Modulus of Nanocomposites Reinforced with Short CNTs in Different Matrices

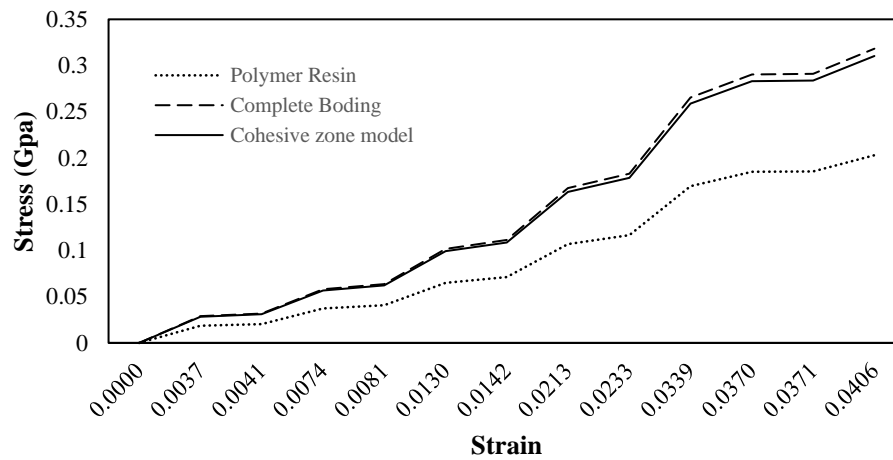


Fig. 12: Stress-Strain Diagram of Short CNTs/Polymer Composite (2% V/V)

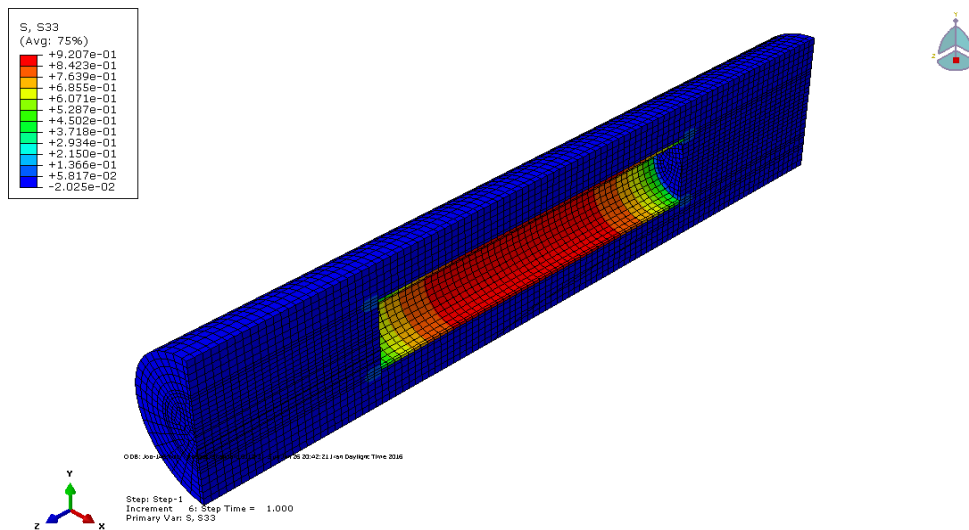


Fig. 13: Stress Transfer in Nanocomposites Reinforced with Short CNTs for $E_f/E_m=200$

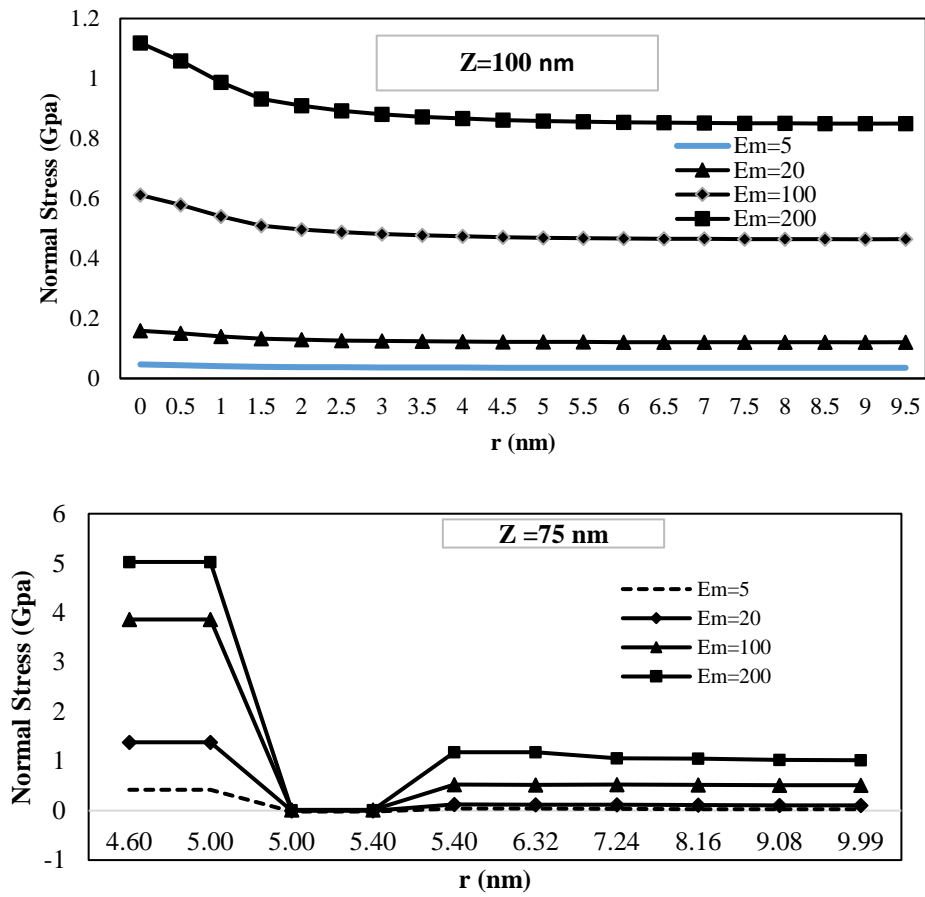


Fig. 14: Variations of Normal Stress Along the Radius of RVE Containing Short CNTs at Z=75 Nm (the Beginning of Fiber) and Z=100 Nm

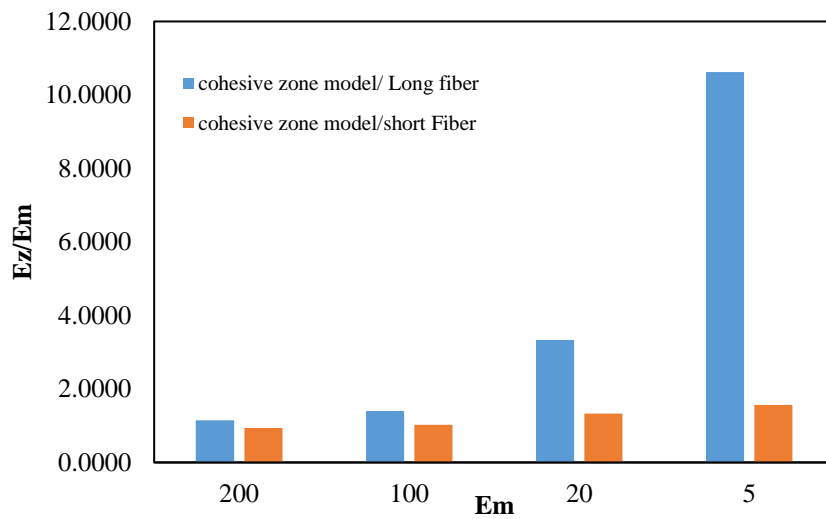


Fig. 15: Comparison of Reinforcement Effect of Short and Long CNTs

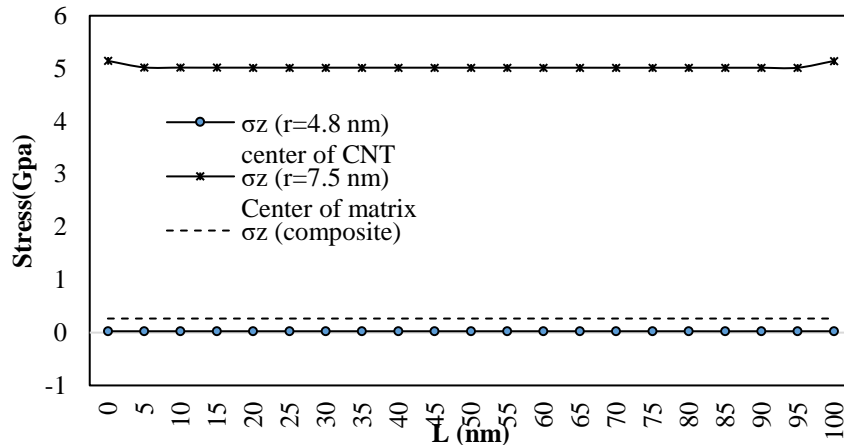


Fig. 16: Normal Stress along the Length of RVE for Nanocomposites Reinforced with Long CNTs

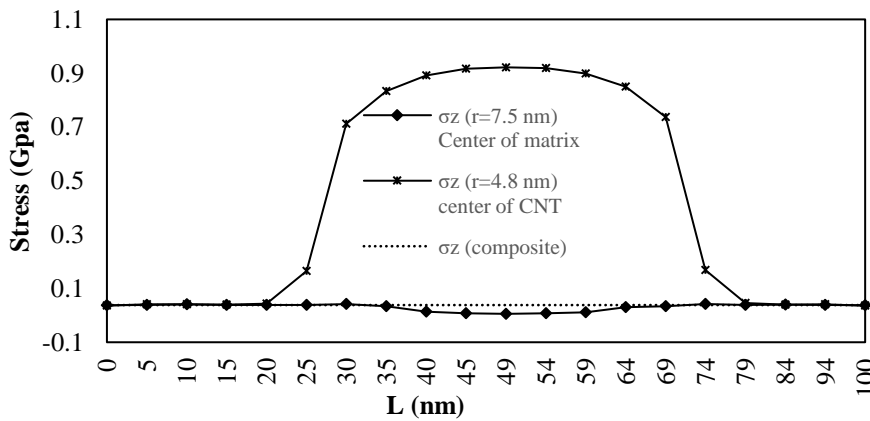


Fig. 17: Normal Stress along the Length of RVE for Nanocomposites Reinforced with Short CNTs

Since the highest tensile stress in the composite is tolerated by CNTs and according to stress law $\sigma_{Composite} = v_{CNT}\sigma_{CNT} + v_m\sigma_m$, the tolerable average stress of fiber was higher than composite stress and average stress of matrix was lower than $\sigma_{Composite}$. This has been shown along the length of RVE and for composites with polymer matrices and reinforced with short and long CNTs in Figs. 16 and 17.

Displacement diagram along the length of RVE for nanocomposites reinforced with short and long CNTs are also shown in Figs. 18 and 19. As can be seen in Fig. 19, at the center of RVE where CNT is located, due to its extremely high elastic modulus, displacement was negligible.

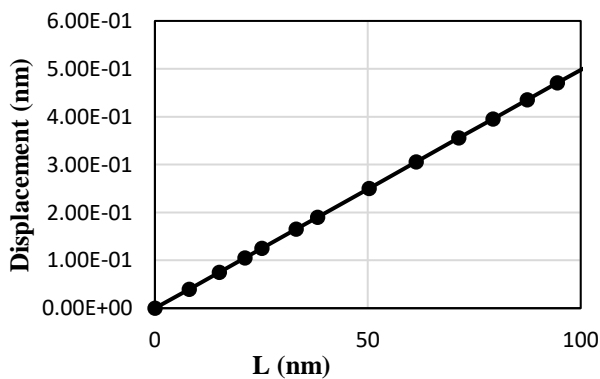


Fig. 18: Displacement Along the Length of RVE for Nanocomposites Reinforced with Long CNTs

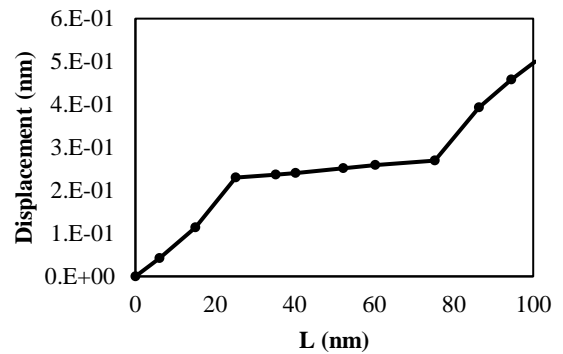


Fig. 19: Displacement along the Length of RVE for Nanocomposites Reinforced with Short CNTs

Shear stress diagram along the length of RVE of polymer/CNTs nanocomposite is shown in Fig. 20. As can be seen, the maximum stress was created on the interface of fiber and matrix and this increased the possibility of slippage in this region. Also, in case of two different shear stresses on the two sides of the border of two different materials, separation occurred.

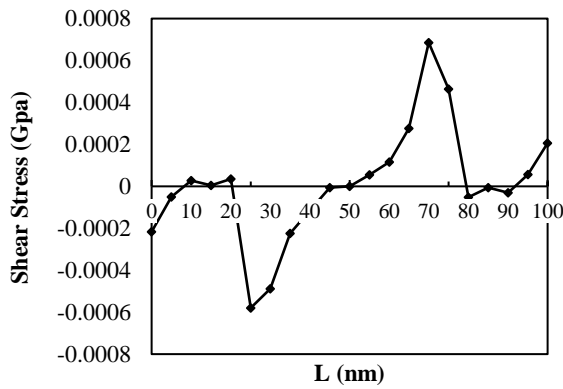


Fig. 20: Shear Stress along the Length of RVE for Nanocomposites Reinforced with Short CNTs (R=5 Nm)

Here, the effects of the addition of CNTs into polyethylene matrix with different weight fractions on compressive and tensile loadings have been investigated. The elastic modulus obtained from this modeling is shown in Table 7 and are compared with experimental results of [33].

Table 7: Experimental and FEM Results for Longitudinal Elastic Modulus (MPa)

Weight fraction	Experimental results	FEM results for tensile loading	FEM results for compressive loading	Difference between models (%)
0.5	2375.7	3050.73	3050.73	28.4
1	3240.9	3990.80	3990.80	23.1
1.5	2642.1	4857.17	4857.17	83.8

According to Fig. 21 and results obtained by modeling, under axial loading, the increase of weight fraction of CNTs significantly increased load transfer capacity from matrix to fiber and therefore the elastic modulus of the nanocomposite. At low weight fractions, model results were well complied with experimental results while at high weight fractions, the difference between results were much higher. Since the dispersion of particles become harder by increasing the volume ratio of CNTs in fabricating samples and performing tests, the experimental results of elastic modulus were lower than those obtained by finite element modeling and even experimental results obtained from lower weight fractions.

Due to their high surface area and very high aspect ratio, CNTs are affected by Van der Waals attractions between themselves which result in their accumulation at high fractions which is called agglomeration. This phenomenon create stress concentration points and failure and prevents sufficient transfer of CNTs properties to polymer matrix. Therefore, obtaining a composition with proper dispersion of CNTs in polyethylene matrix has always been among the most important factors in achieving a good nanocomposite composition.

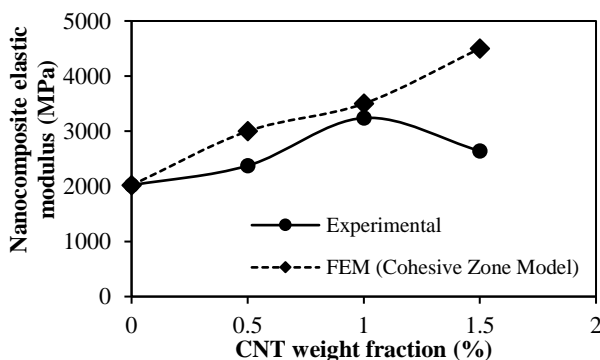


Fig. 21: The Effect of CNT Weight Fraction on Polyethylene/CNT Nanocomposite Elastic Modulus

The effect of the addition of CNTs into nanocomposites with polyethylene matrix under compressive loading at different weight fractions have been investigated. As can be seen in Fig. 23, the addition of SWCNTs into polyethylene matrices had similar effects under tensile and compressive loadings while the addition of MWSNTs was more effective under compressive loadings than tensile loadings. During tensile loading, since the load was not transferred onto inner layers, no slippage occurred among the layers of MWCNTs, but under compressive loading, the load was transferred onto inner layers of MWCNTs and therefore, the effectiveness of MWCNTs was higher under compressive loadings [33].

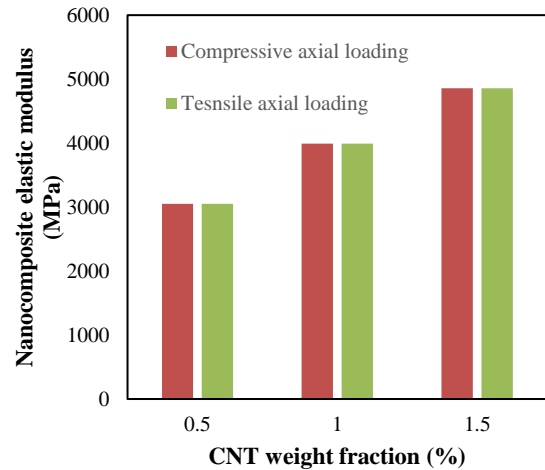


Fig. 22: Comparison of the Effect of the Addition of CNTs on Tensile and Compressive Axial Loadings

The unique properties of CNTs depend on their atomic arrangement, length, diameter and structure and among them the aspect ratio (the ratio of length to diameter) of CNTs has a significant effect on the average load transfer value of CNTs. In nanocomposites reinforced with CNTs, the length of CNTs can reach 20 μm . Recently, CNTs 1 cm in length have been fabricated. Since the diameter of CNTs can change a few nanometers, at constant weight fraction and diameter of CNTs, the elastic modulus of volume elements for different CNTs lengths have been calculated which are shown in Fig. 23.

At shorter lengths of CNTs, fiber did not have reinforcement effect and could not compensate material shortage due to the replacement of CNTs. By increasing the length or aspect ratio of CNTs, longitudinal elastic modulus of nanocomposite was increased.

Therefore, in finite element RVE modeling, instead of modeling the whole length of CNT, once can model only a part of it. Also, according to Fig. 25, in the modeling of CNTs for RVE, the length of CNTs was chosen such that the reinforcement effect of fiber was guaranteed.

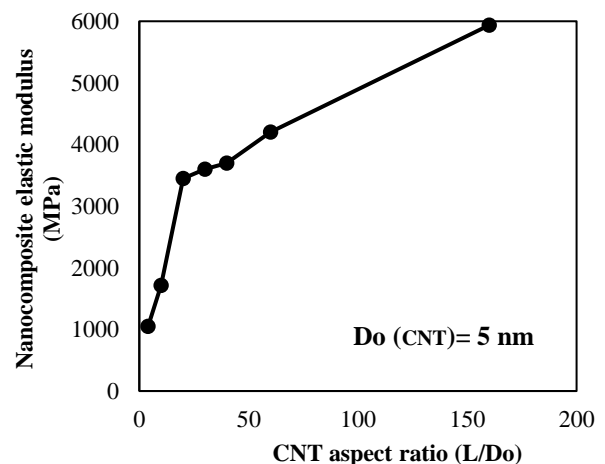


Fig. 23: The Effect of the CNT Aspect Ratio on the Elastic Modulus of Polyethylene/CNTs Nanocomposite

According to the fact that the wall thickness of CNTs is equal to the thickness of graphene and is 3.4Å, it was assumed that carbon atoms were located in the central circle of this thickness. Also, resin could not penetrate into CNTs and the innermost resin layer touched the outer surface of CNTs. Therefore, the minimum thickness of intermediate phase was 1.7 Å [34]. Depending on the quality of the attachment of CNTs to resin, this value could increase. Fig. 21 shows the effect of interface thickness on the longitudinal elastic moduli of polyethylene/CNTs (1% w/w) nanocomposite. It can be seen that by increasing the thickness of intermediate phase, the hardness of the attachment was increased and Young's modulus began to increase. In fact, by decreasing the thickness of intermediate phase, the effective forces between CNTs and resin atoms were decreased and by the weakening of these attachments, load transfer from resin to CNTs did not occur properly.

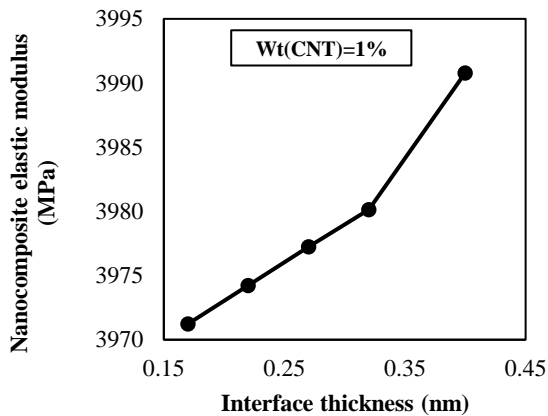


Fig. 24: The Effect of Interface Thickness on the Elastic Modulus of Polyethylene/CNTs Nanocomposite

Two states of total stress transfer from intermediate phase and lack of stress transfer between matrix and fiber were boundary states of load transfer from intermediate phase. In other words, without load transfer, elastic modulus of nanocomposites were equal to those of matrix. The hardness of composite increases with the increase of the hardness of intermediate phase and therefore the capacity of stress transfer; therefore, at complete load transfer, the elastic modulus of intermediate had the highest possible value. This is shown in Fig. 27 for different weight fractions. When the number of chemical bonds between matrix and CNTs was high, the elastic modulus of intermediate phase was about 5 GPa and this was related to the ideal state of load transfer from matrix to CNTs. On the other hand, when elastic modulus of intermediate phase was about 5 MPa, the elastic modulus of composite was close to that of matrix.

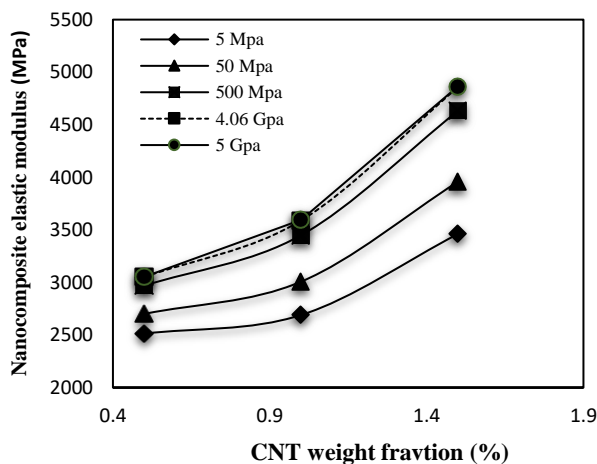


Fig. 25: The Effect of the Strength of Intermediate Phase on the Elastic Modulus of Polyethylene/CNTs Nanocomposite.

Fig. 23 shows the effect of the variations of elastic modulus of matrix on that of composite in different intermediate phases. The elastic modulus of polymer was generally 1-10 GPa. As can be seen in the figure, the elastic modulus of composite increased by the increase of the hardness of matrix and decreases by the decrease of intermediate phase.

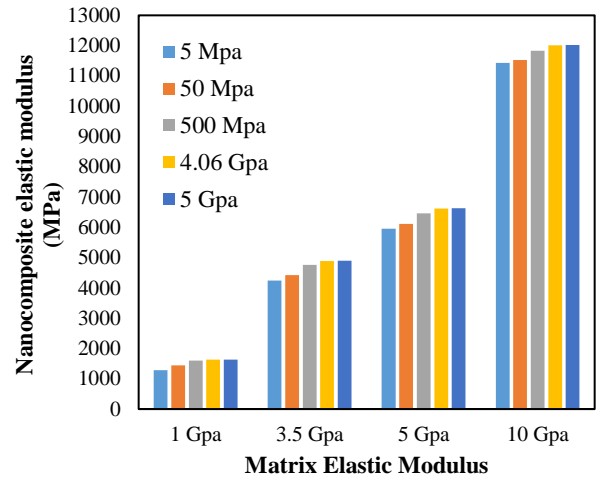


Fig. 26: The Effect of the Hardness of Matrix on the Elastic Modulus of Nanocomposite

Fig. 27 shows the effect of the elastic modulus of fiber on that of composite with polyethylene matrix in terms of different values of interface hardnesses. The values of elastic modulus for glass, carbon, silicon carbide, and CNTs fibers were assumed to be 85, 300, 400, and 1000 GPa, respectively. Composites reinforced with CNTs fibers had extremely higher tensile properties and very higher hardnesses compared to other composites reinforced with other reinforcers. For example, if interface hardness was assumed to be 50 MPa for common polymer-CNTs bandings, by adding 0.5% w/w fiber into matrix, the reinforcement ability of CNTs compared to normal fiber carbon was increased by 10%. Therefore, Fig. 27 proves the high potential of CNTs compared to other fibers to be used for increasing tensile strength of composites with polyethylene matrix.

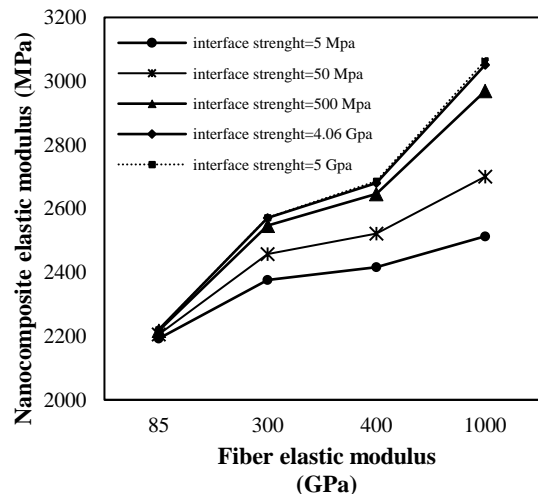


Fig. 27: The Effect of Fiber Elastic Modulus on Nanocomposite Elastic Modulus for Different Interface Strength (Wt = 0.5%).

4. Concluding remarks

This study aimed to evaluate the mechanical properties of SWCNTs-reinforced composites using 3-D representative volume element (RVE). Then, RVE was created by finite element method using ABAQUS software and its elastic behavior was simulated.

By using the results of atomic modeling, fiber and matrix interface properties were extracted and a model for predicting the elastic modulus of e nanocomposites was presented.

The effects of geometric and mechanical properties of fiber, matrix and interface on elastic modulus, displacement and stresses of nanocomposite were investigated.

References

- [1] Qian, D., Liu, W.K., Ruoff, R.S. (2001). Mechanics of C60 in nanotubes, *Phys Chem B* 105, 10753–10758. <https://doi.org/10.1021/jp0120108>.
- [2] Coleman, J.N., Khan, U., Blau, W.J., Gun'ko, Y.K. (2006). Small but strong: a review of the mechanical properties of carbon nanotube-polymer composites, *Carbon* 44(9), 1624–1652. <https://doi.org/10.1016/j.carbon.2006.02.038>.
- [3] Azizi, S., Fattahi, A.M., Waj, N. (2018). Investigation of elastic properties of PE/CNT injected composites, *International Journal of Engineering and Technology (UAE)* 7(4), 3330–3334.
- [4] Thostenson, E.T., Ren, Z., Chou, T-W. (2001). Advances in the science and technology of carbon nanotubes and their composites: a review, *Composite Science and Technology* 61(13), 1899–1912. [https://doi.org/10.1016/S0266-3538\(01\)00094-X](https://doi.org/10.1016/S0266-3538(01)00094-X).
- [5] Safaei, B., Fattahi, A.M., Chu, F. (2018). Finite element study on elastic transition in platelet reinforced composites, *Microsystem Technologies* 24(6), 2663–2671. <https://doi.org/10.1007/s00542-017-3651-y>.
- [6] Andrews, R., Jacques, D., Minot, M., Rantell, T. (2002). Fabrication of carbon multiwall nanotube/polymer composites by shear mixing, *Macromolecular Materials Engineering* 287(6), 395–403. [https://doi.org/10.1002/1439-2054\(20020601\)287:6<395::AID-MAME395>3.0.CO;2-S](https://doi.org/10.1002/1439-2054(20020601)287:6<395::AID-MAME395>3.0.CO;2-S).
- [7] Safaei, B., Moradi-Dastjerdi, R., Qin, Z., Chu, F. (2019). Frequency-dependent forced vibration analysis of nanocomposite sandwich plate under thermo-mechanical loads, *Composites Part B: Engineering* 161, 44–54. <https://doi.org/10.1016/j.compositesb.2018.10.049>.
- [8] Safaei, B., Moradi-Dastjerdi, R., Chu, F. (2018). Effect of thermal gradient load on thermo-elastic vibrational behavior of sandwich plates reinforced by carbon nanotube agglomerations, *Composite Structures* 192, 28–37. <https://doi.org/10.1016/j.compstruct.2018.02.022>.
- [9] Joshi, U.A., Sharma, S.C., Harsha, S.P. (2011). Analysis of elastic properties of carbon nanotube reinforced nanocomposites with pinhole defects, *Computational Materials Science* 50(11), 3245–3256. <https://doi.org/10.1016/j.commatsci.2011.06.011>.
- [10] Safaei, B., Naseradinmousavi, P., Rahmani, A. (2016). Development of an accurate molecular mechanics model for buckling behavior of multi-walled carbon nanotubes under axial compression, *Journal of Molecular Graphics and Modelling* 65, 43–60. <https://doi.org/10.1016/j.jmgm.2016.02.001>.
- [11] Liu, Y.J., Chen, X.L. (2003). Evaluations of the effective material properties of carbon nanotube-based composites using a nanoscale representative volume element, *Mechanics of Materials* 35, 69–81. [https://doi.org/10.1016/S0167-6636\(02\)00200-4](https://doi.org/10.1016/S0167-6636(02)00200-4).
- [12] Joshi, P., Upadhyay, S.H. (2014). Evaluation of elastic properties of multi walled carbon nanotube reinforced composite, *Computational Materials Science* 81, 332–338 <https://doi.org/10.1016/j.commatsci.2013.08.034>.
- [13] Azizi, S., Fattahi, A.M., Kahnemouei, J.T. (2015). Evaluating mechanical properties of nanoplatelet reinforced composites under mechanical and thermal loads, *Journal of Computational and Theoretical Nanoscience* 52(12), 1–7. <https://doi.org/10.1166/jctn.2015.4334>.
- [14] Roozpekar, S., Fattahi, A.M. (2019). Evaluation of elastic modulus in PE/CNT composites subjected to axial loads, *SN Applied Sciences* 1: 17. <https://doi.org/10.1007/s42452-018-0022-y>
- [15] Fattahi, A.M., Sahmani, S. (2017). Size dependency in the axial post-buckling behavior of nanopanels made of functionally graded material considering surface elasticity, *Arabian Journal for Science and Engineering* 42, 1–17. <https://doi.org/10.1007/s13369-017-2600-5>.
- [16] Moradi-Dastjerdi, R., Aghadavoudi, F. (2018) Static analysis of functionally graded nanocomposite sandwich plates reinforced by defected CNT, *Composite Structures* 200, 839–848. <https://doi.org/10.1016/j.compstruct.2018.05.122>.
- [17] Moradi-Dastjerdi, R., Payganeh, G. (2018). Thermoelastic vibration analysis of functionally graded wavy carbon nanotube-reinforced cylinders, *Polymer Composites* 39, E826–E834. <https://doi.org/10.1002/pc.24278>.
- [18] Hosseini, R., Zargar, O., Hamed, M. (2018). Improving Power Density of Piezoelectric Vibration-Based Energy Scavengers, *Journal of Solid Mechanics* 10(1), 98–109.
- [19] Mohammadsalehi, M., Zargar, O., Baghani, M. (2017). Study of non-uniform viscoelastic nanoplates vibration based on nonlocal first-order shear deformation theory, *Meccanica*, 52(4-5), 1063–1077. <https://doi.org/10.1007/s11012-016-0432-0>.
- [20] Sahmani, S., Fattahi, A.M. (2017). Nonlocal size dependency in non-linear instability of axially loaded exponential shear deformable FG-CNT reinforced nanoshells under heat conduction, *The European Physical Journal plus* 132 (5), 231. <https://doi.org/10.1140/epjp/i2017-11497-5>.
- [21] Sahmani, S., Fattahi, A.M. (2016). Size-dependent nonlinear instability of shear deformable cylindrical nanopanels subjected to axial compression in thermal environments, *Microsystem Technologies* 23 (10), 4717–4731. <https://doi.org/10.1007/s00542-016-3220-9>.
- [22] Sahmani, S., Fattahi, A.M. (2017). Imperfection sensitivity of the size-dependent nonlinear instability of axially loaded FGM nanopanels in thermal environments, *Acta Mechanica* 228 (11), 3789–3810. <https://doi.org/10.1007/s00707-017-1912-6>.
- [23] Sahmani, S., Fattahi, A.M. (2017). An anisotropic calibrated non-local plate model for biaxial instability analysis of 3D metallic carbon nanosheets using molecular dynamics simulations, *Materials Research Express* 4(6), 1–14. <https://doi.org/10.1088/2053-1591/aa6bc0>.
- [24] Sahmani, S., Fattahi, A.M. (2017). Calibration of developed nonlocal anisotropic shear deformable plate model for uniaxial instability of 3D metallic carbon nanosheets using MD simulations, *Computer Methods in Applied Mechanics and Engineering* 322, 187–207. <https://doi.org/10.1016/j.cma.2017.04.015>.
- [25] Sahmani, S., Fattahi, A.M. (2017). Development an efficient calibrated nonlocal plate model for nonlinear axial instability of zirconia nanosheets using molecular dynamics simulation, *Journal of Molecular Graphics and Modelling* 75, 20–31. <https://doi.org/10.1016/j.jmgm.2017.04.018>.
- [26] Huang, Z., Qin, Z., Chu, F. (2016). Damping mechanism of elastic-viscoelastic-elastic sandwich structures, *Composite Structures* 153, 96–107. <https://doi.org/10.1016/j.compstruct.2016.05.105>.
- [27] Huang, Z., Qin, Z., Chu, F. (2016). A comparative study of finite element modeling techniques for dynamic analysis of elastic-viscoelastic-elastic sandwich structures, *Journal of Sandwich Structures and Materials* 18(5), 531–551. <https://doi.org/10.1177/1099636215623091>.
- [28] Huang, Z., Qin, Z., Chu, F. (2016). Vibration and damping characteristics of sandwich plates with viscoelastic core, *JVC/Journal of Vibration and Control* 22(7), 1876–1888. <https://doi.org/10.1177/1077546314545527>.
- [29] Huang, Z., Qin, Z., Chu, F. (2018). A compression shear mixed finite element model for vibration and damping analysis of viscoelastic sandwich structures, *Journal of Sandwich Structures and Materials*. <https://doi.org/10.1177/1099636218794576>.
- [30] Moradi-Dastjerdi, R., Malek-Mohammadi, H. (2017). Biaxial buckling analysis of functionally graded nanocomposite sandwich plates reinforced by aggregated carbon nanotube using improved high-order theory, *Journal of Sandwich Structures and Materials* 19(6), 736–769. <https://doi.org/10.1177/1099636216643425>.
- [31] Moradi-Dastjerdi, R., Malek-Mohammadi, H., Momeni-Khabisi, H. (2016). Free vibration analysis of nanocomposite sandwich plates reinforced with CNT aggregates, *ZAMM Zeitschrift für Angewandte Mathematik und Mechanik* 97(11), 1418–1435.
- [32] Moradi-Dastjerdi, R., Momeni-Khabisi, H. (2018). Vibrational behavior of sandwich plates with functionally graded wavy carbon nanotube-reinforced face sheets resting on Pasternak elastic foundation, *JVC/Journal of Vibration and Control* 24(11), 2327–2343. <https://doi.org/10.1177/1077546316686227>.
- [33] Najipour, A., Fattahi, A.M. (2017). Experimental study on mechanical properties of PE/CNT composites, *J Theor Appl Mech* 55(2), 719–726. <https://doi.org/10.15632/jtam-pl.55.2.719>.
- [34] Namilae, S., Chandra, N. (2005). Multiscale model to study the effect of interfaces in carbon nanotube-based composites, *Journal of Engineering Materials and Technology* 127(2), 222–232. <https://doi.org/10.1115/1.1857940>.
- [35] Fattahi, A.M., Safaei, B. (2017). Buckling analysis of CNT-reinforced beams with arbitrary boundary conditions, *Microsystem Technologies* 23(10), 5079–5091. <https://doi.org/10.1007/s00542-017-3345-5>.
- [36] Sahmani, S., Fattahi, A.M. (2017). Thermo-electro-mechanical size-dependent postbuckling response of axially loaded piezoelectric

- shear deformable nanoshells via nonlocal elasticity theory, *Microsystem Technologies* 23(10), 5105–5119. <https://doi.org/10.1007/s00542-017-3316-x>.
- [37] Fattahi, A.M., Sahmani, S. (2017). Nonlocal temperature-dependent postbuckling behavior of FG-CNT reinforced nanoshells under hydrostatic pressure combined with heat conduction, *Microsystem Technologies* 23(10), 5121–5137. <https://doi.org/10.1007/s00542-017-3377-x>.
- [38] Azizi, S., Safaei, B., Fattahi, A.M., Tekere, M. (2015). Nonlinear vibrational analysis of nanobeams embedded in an elastic medium including surface stress effects, *Advances in Materials Science and Engineering* 2015, 1–7. <https://doi.org/10.1155/2015/318539>.
- [39] Ghanati, P., Safaei, B. (2018). Elastic buckling analysis of polygonal thin sheets under compression, *Indian Journal of Physics* 2018:6. <https://doi.org/10.1007/s12648-018-1254-9>.
- [40] Sahmani, S., Fattahi, A.M. (2018). Small scale effects on buckling and postbuckling behavior of axially loaded FGM nanoshells based on nonlocal strain gradient elasticity theory, *Applied Mathematics and Mechanics* 39(4), 561–580. <https://doi.org/10.1007/s10483-018-2321-8>.
- [41] Moradi-Dastjerdi, R., Payganeh, G., Tajdari, M. (2017). Resonance in functionally graded nanocomposite cylinders reinforced by wavy carbon nanotube, *Polymer Composites* 38, E542-E552. <https://doi.org/10.1002/pc.24045>.
- [42] Gu, L., Qin, Z., Chu, F. (2015). Analytical analysis of the thermal effect on vibrations of a damped Timoshenko beam, *Mechanical Systems and Signal Processing* 60–61, 619–643. <https://doi.org/10.1016/j.ymsp.2014.11.014>.
- [43] Moradi-Dastjerdi, R., Payganeh, G. (2017). Transient heat transfer analysis of functionally graded CNT reinforced cylinders with various boundary conditions, *Steel and Composite Structures* 24(3), 359–367.
- [44] Sahmani, S., Fattahi, A.M. (2017). Development of efficient size-dependent plate models for axial buckling of single-layered graphene nanosheets using molecular dynamics simulation, *Microsystem Technologies* 24(2), 1265–1277. <https://doi.org/10.1007/s00542-017-3497-3>.
- [45] Qin, Z., Chu, F., Zu, J. (2017). Free vibrations of cylindrical shells with arbitrary boundary conditions: A comparison study, *International Journal of Mechanical Sciences* 133, 91–99. <https://doi.org/10.1016/j.ijmecsci.2017.08.012>.
- [46] Moheimani, R., Hasansade, M. (2018). A closed-form model for estimating the effective thermal conductivities of carbon nanotube–polymer nanocomposites, *Proceedings of the Institution of Mechanical Engineers, Part C: Journal of Mechanical Engineering Science* 0, 1–11. <https://doi.org/10.1177/0954406218797967>.
- [47] Qin, Z., Yang, Z., Zu, J., Chu, F. (2018). Free vibration analysis of rotating cylindrical shells coupled with moderately thick annular plates, *International Journal of Mechanical Sciences* 142–143, 127–139. <https://doi.org/10.1016/j.ijmecsci.2018.04.044>.
- [48] Safaei, B., Fattahi, A.M. (2017). Free Vibrational Response of Single-Layered Graphene Sheets Embedded in an Elastic Matrix using Different Nonlocal Plate Models, *MECHANIKA* 23(5), 678–687. <http://dx.doi.org/10.5755/j01.mech.23.5.14883>
- [49] Damadam, M., Moheimani, R., Dalir, H. (2018). Bree’s diagram of a functionally graded thick-walled cylinder under thermomechanical loading considering nonlinear kinematic hardening, *Case Studies in Thermal Engineering* 12, 644–54. <https://doi.org/10.1016/j.csite.2018.08.004>.
- [50] Sahmani, S., Fattahi, A.M., Ahmed, N.A. (2018). Analytical mathematical solution for vibrational response of postbuckled laminated FG-GPLRC nonlocal strain gradient micro-/nanobeams, *Engineering with Computers*, 1–17. <https://doi.org/10.1007/s00366-018-0657-8>.
- [51] Sahmani, S., Fattahi, A.M., Ahmed, N.A. (2018). Nonlinear torsional buckling and postbuckling analysis of cylindrical silicon nanoshells incorporating surface free energy effects, *Microsystem Technologies* 1–14. <https://doi.org/10.1007/s00542-018-4246-y>